LETTERS
PUBLISHED ONLINE: 11 NOVEMBER 2012 | DOI: 10.1038/NGEO1627
nature geoscience

Wind-driven trends in Antarctic sea-ice drift

Paul R. Holland[1]* and Ron Kwok[2]

The sea-ice cover around Antarctica has experienced a slight expansion in area over the past decades[1,2]. This small overall increase is the sum of much larger opposing trends in different sectors that have been proposed to result from changes in atmospheric temperature or wind stress[3–5], precipitation[6,7], ocean temperature[8], and atmosphere or ocean feedbacks[9,10]. However, climate models have failed to reproduce the overall increase in sea ice[11]. Here we present a data set of satellite-tracked sea-ice motion for the period of 1992–2010 that reveals large and statistically significant trends in Antarctic ice drift, which, in most sectors, can be linked to local winds. We quantify dynamic and thermodynamic processes in the internal ice pack and show that wind-driven changes in ice advection are the dominant driver of ice-concentration trends around much of West Antarctica, whereas wind-driven thermodynamic changes dominate elsewhere. The ice-drift trends also imply large changes in the surface stress that drives the Antarctic ocean gyres, and in the fluxes of heat and salt responsible for the production of Antarctic bottom and intermediate waters.

Satellite studies of Antarctic sea-ice motion[12–14] have greatly advanced our understanding of its large-scale dynamics, but their short length and combination of different sensors have precluded an investigation of decadal ice-motion trends. We present a new consistent data set for April–October 1992–2010 that is specifically designed to address this question (see Methods). The long-term mean of these ice-motion data is in good agreement with shorter data sets reported previously[12–14]. Away from coastlines, the ice is close to a state of free drift, moving at a small (spatially variable) angle to the left of the geostrophic wind[14], which follows contours of atmospheric pressure (Fig. 1a). This creates a tendency for the ice to circulate around the three climatological lows in the circumpolar pressure trough that surrounds Antarctica, leading to maximum ice export in the Weddell, Cooperation and Ross seas. A nearly continuous westward current dominates ice flow next to the coast.

The freely drifting areas have a strong correlation between ice motion and winds[14]. Figure 1b shows a map of the vector correlation between interannual time series of April–October mean ice motion and 10-m winds from the ERA-Interim atmospheric reanalysis (see Methods). The spatial mean of the correlations is $r^2 = 0.52$, but large areas in the Pacific and Atlantic sectors have $r^2 > 0.7$. This quantifies the effect of winds on ice motion through both direct wind stress and any portion of the ocean stress and sea-surface tilt forcing that is correlated to local winds. The remaining ice-motion variance can be attributed to error in the motion-tracking and atmosphere reanalysis model, ocean forcing decorrelated from local winds, and modification of ice motion by internal stresses. Low-correlation areas in Fig. 1b are generally associated with convergent ice motion or flow near coastlines, where internal stresses are large.

Our primary advance is the discovery of large and spatially variable decadal trends in ice motion (Fig. 2a), with statistically significant ice-speed changes (trend multiplied by period) of up to 30% occurring over 19 years. Changes in the meridional component of ice motion, which is largely responsible for the size and shape of the Antarctic ice cover, are even greater. Widespread increases of $\sim$2 cm s^{-1} in northward export in the Ross and Amundsen seas equal the mean northward drift during this period ($\sim$2 cm s^{-1}), and similar northward changes ($\sim$2 cm s^{-1}) occur in the Kong Håkon VII Hav (mean $\sim$4 cm s^{-1}; King Håkon Sea hereafter). In contrast, northward ice export in the Weddell Sea decreased by $\sim$1 cm s^{-1} (mean $\sim$4 cm s^{-1}), focused on a strong and significant decrease in export from the Ronne Polynya in the southwest. Bellingshausen Sea ice experienced a large but insignificant change of $\sim$3 cm s^{-1} southward, implying great variability around its mean of $\sim$1 cm s^{-1} northward. Opposing ice-drift trends in the Ross and Bellingshausen seas have been inferred previously from atmospheric model winds[4,15], but are observed and quantified here for the first time. Changed ice motion in the southernmost Ross and Weddell seas has been shown to affect dense-water formation over limited regions[16,17] but our data reveal widespread and coherent drift anomalies north of the near-shore polynyas.

The strong correlation between observed ice motion and reanalysis winds in most of the sea-ice zone implies that ice-motion trends are largely caused by wind trends (Fig. 2b). In fact, the correlations in Fig. 1b specifically quantify this linkage because they are calculated between the data sets used to calculate the trends shown in Fig. 2 (see Methods). Modelled surface pressure trends suggest that opposing changes in the Ross and Bellingshausen seas are responding to a large but statistically insignificant reduction in pressure centred on the Amundsen Sea, whereas changes in the Weddell and King Håkon seas are caused by a smaller but significant increase in pressure over the prime meridian. The high correlations cross-validate the ice motion tracking and reanalysis model in these regions. Agreement between the trends is poorer around East Antarctica, as expected given the proximity of the ice to the coast in this region. However, some disagreements, such as that in the Mawson Sea, are large enough to imply that the ice-motion data or reanalysis winds may be erroneous.

The ice-motion trends provide new insight into the well-known but poorly understood changes in Antarctic ice concentration. Concentration trends are largest in autumn[1,2,4,9], and geographical trend patterns persist largely unaltered until spring[18]. This suggests that most winter anomalies emanate from large changes in the autumn ice-edge advance, possibly as a result of summertime ice–ocean feedbacks[9,19]. Autumn concentration trends for 1992–2010 (Fig. 3a) mimic those described previously for the full post-1978 satellite record[4,18], with large losses at the ice edge in the Bellingshausen and Mawson ($\sim$2% yr^{-1}) and Weddell ($\sim$1% yr^{-1}) seas outweighed by widespread gains in the Ross ($\sim$1% yr^{-1}) and King Håkon and Cosmonaut ($\sim$0.5% yr^{-1}) seas. Overlaying ice-motion trend vectors onto these changes suggests a link, with regions of significantly increased northward ice flow exhibiting significant increases in ice concentration and vice versa. This link seems strongest in the Atlantic and Pacific sectors, notably failing in the Mawson Sea. Figure 3b shows a strong and significant autumn

[1]British Antarctic Survey, Cambridge CB3 0ET, UK, [2]Jet Propulsion Laboratory, California Institute of Technology, Pasadena, California 91109, USA.
*e-mail: p.holland@bas.ac.uk.

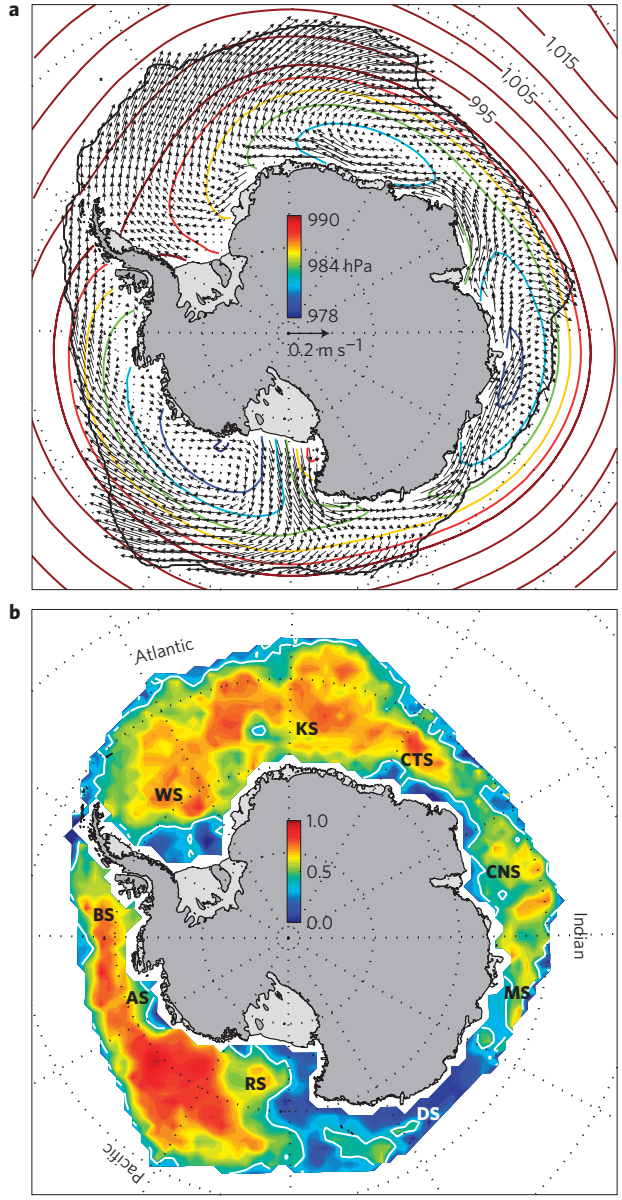

Figure 1 | April–October 1992–2010 mean ice motion and its relation to wind forcing. Wind and ice motion are strongly coupled in Pacific and Atlantic sectors but weakly related around East Antarctica, where a coastal current of ice dominates. **a**, Mean ice-motion vectors overlaid on ERA-Interim reanalysis sea-level pressure. **b**, Vector correlation between ice-motion vectors and ERA-Interim 10-m wind vectors (white contours show $r^2 = 0.4$, significant at 99%). WS, Weddell Sea; KS, King Håkon Sea; CTS, Cosmonaut Sea; CNS, Cooperation Sea; MS, Mawson Sea; DS, Dumont D'Urville Sea; RS, Ross Sea; AS, Amundsen Sea; BS, Bellingshausen Sea.

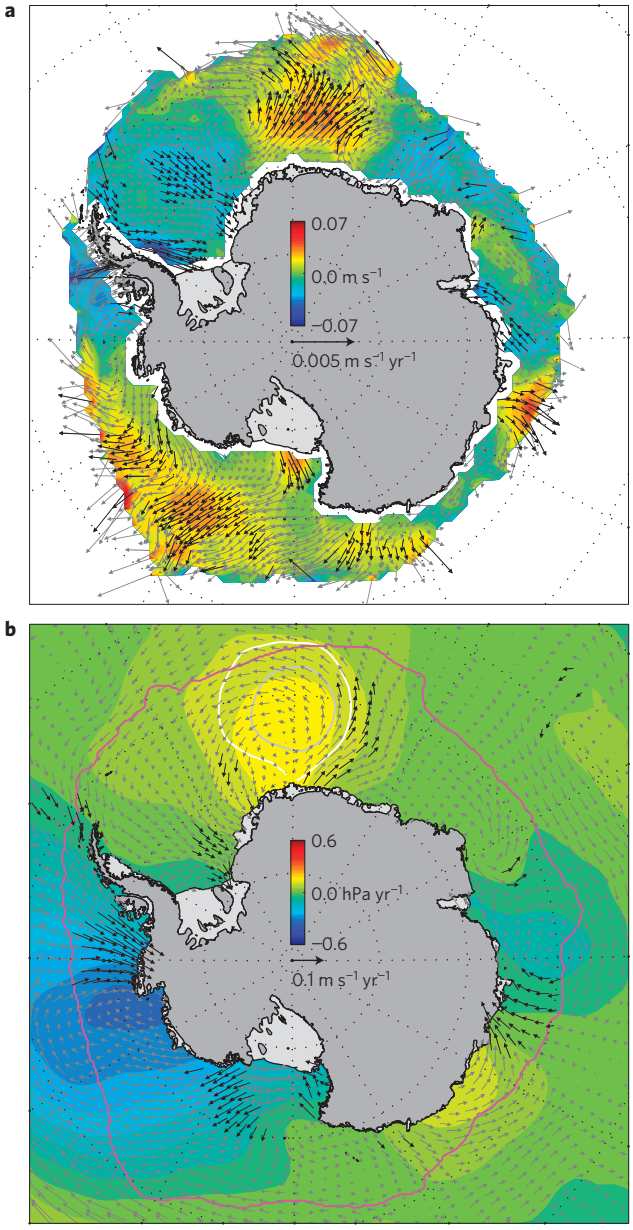

Figure 2 | April–October 1992–2010 ice-motion trends and their relation to wind forcing. Large and statistically significant changes in ice motion are driven by changes in the winds. **a**, Ice-motion trend vectors overlaid on 19-year change in meridional ice speed (change is linear trend multiplied by period, positive northwards; black vectors have meridional ice-motion trends significant at >90%). **b**, ERA-Interim reanalysis 10-m wind trend vectors overlaid on trend in sea-level pressure (white and grey contours show pressure trends significant at 90% and 95%; black vectors have meridional wind trends significant at >90%; magenta contour shows extent of motion trends).

deepening over the Amundsen Sea, thought to result from the increased intensity of the Southern Annular Mode[4,5,15]. Autumn ice-motion trends are again closely related to wind trends in the Atlantic and Pacific sectors and disagree elsewhere. A significant trend towards northerly winds occurs in the Mawson Sea, suggesting a wind-driven decrease in ice concentration that is not reflected in ice-motion trends.

The general link between trends in ice concentration and ice motion or winds seems strong. However, this cannot separate dynamic from thermodynamic causes, because more southerly winds could increase the ice concentration through either increased transport of ice from the south or through an atmospheric cooling from increased advection of cold polar air masses[3–5]. Similarly, more northerly winds would decrease ice transport and cause atmospheric warming. Our new data present a unique opportunity to quantify these processes by decomposing the ice-concentration budget in the internal ice pack into dynamic and thermodynamic contributions. The ice concentration change and its dynamic contribution are calculated by combining concentration and motion data, and their residual is found to represent the thermodynamic contribution (see Supplementary Methods).

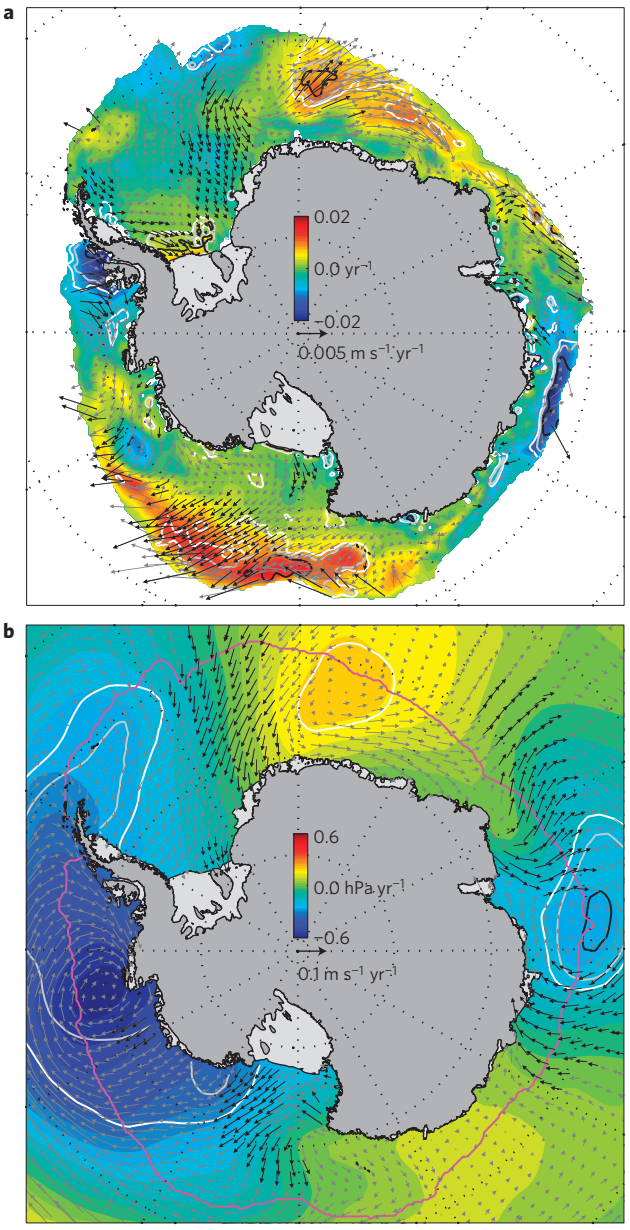

Figure 3 | Autumn (April–June) 1992–2010 ice motion and concentration trends and their relation to wind forcing. Wind-driven changes in ice motion are clearly linked to changes in ice concentration. **a**, Ice-motion trend vectors overlaid on ice-concentration trends. **b**, ERA-Interim 10-m wind trend vectors overlaid on trend in sea-level pressure. White, grey and black contours show underlay field trends significant at 90%, 95% and 99% respectively; black vectors have meridional trends significant at >90%; magenta contour in **b** shows extent of concentration trends.

Before examining trends, it is instructive to first decompose the mean April–October ice-concentration budget[20] (Supplementary Fig. S1). Freezing in the inner pack is maintained by divergence, which supports greater ocean–atmosphere heat exchange than is otherwise possible in consolidated ice. In the main export regions, ice is advected to the margins and then melted, because it is thermodynamically unsustainable there even in winter; the ice cover in these regions extends hundreds of kilometres further equatorward than it would in the absence of northward advection. This illustrates the Antarctic sea-ice freshwater pump, which contributes brine to Antarctic Bottom Water close to the continent and fresh water to Antarctic Intermediate Water and mode waters in the ice-melting zone. In areas of mean northerly winds (Bellingshausen, Cosmonaut and Dumont D'Urville seas; Fig. 1a) southward advection opposes thermodynamic growth of the ice cover, and freezing extends closer to the ice edge.

The mean concentration difference over autumn is dominated by freezing, with advection and divergence being minor contributors during this period (Supplementary Fig. S2). However, in the Pacific sector and Weddell Sea, trends in the autumn concentration difference seem to be strongly influenced by dynamics (Supplementary Fig. S3). In contrast, trends in the King Håkon Sea are controlled by thermodynamics. Supplementary Fig. S4 shows the proportion of the autumn concentration difference trend that is explained by trends in dynamical processes. The ratio is noisy, but after heavy smoothing, it confirms that dynamic trends dominate in the Pacific sector. Trends in freezing in this sector can actually oppose the ice-concentration changes, because dynamical processes are progressively replacing thermodynamics. Ice-concentration losses in the Weddell Sea also seem to be caused by decreased northward advection, but the concentration increase in King Håkon Sea and other changes around East Antarctica contain a strong thermodynamic component. The wind trends in these regions suggest that changes in cold- and warm-air advection explain the thermodynamic trends.

The ultimate cause of the wind and ice changes lies in the large-scale climate variability of the Southern Hemisphere. Antarctic sea ice can contain 3–5-year cyclic anomalies that might be partly aliased into our calculations[1,16,21], but our trends cover several such cycles and are consistent with longer-term studies[18]. Aspects of the wind trends (and therefore ice-motion trends) can be attributed to large-scale modes such as the Southern Annular Mode and El Niño/Southern Oscillation[3,19,22]. Modern trends in these modes could arise through natural variability, but some evidence suggests that they are forced by the Southern Hemisphere ozone hole and increased greenhouse gases[4,23]. Our conclusions that ice-motion trends are dominated by winds, and that winds contribute significantly to ice concentration trends through both dynamic and thermodynamic effects, reinforce the need for a better understanding of both the wind changes and the anthropogenic forcing of relevant climate modes.

Our conclusions are of fundamental importance in rectifying the failure of present climate models to hindcast the recent increase in Antarctic sea ice[11]. In particular, they suggest that surface winds and ice dynamics and thermodynamics must be accurately represented. Our data set provides an observational map of changes against which models can be compared, and any faults can be diagnosed using our decomposition of the ice-concentration budget into dynamic and thermodynamic components. When climate models can hindcast ice-concentration increases we will have good reason to believe their forecasted ice loss under the effects of climate change.

Our data offer a new view of surface change relevant to all components of the Antarctic climate. The good fit between ice motion and reanalysis wind trends, in an area of extremely sparse *in situ* data, is testament to the power of satellite sounder data assimilation into ERA-Interim. It also implies confidence that these winds can be used to force models of Antarctic ice and ocean trends over recent decades. The large and widespread changes in ice motion imply considerable changes in sea-surface forcing, both directly through observed changes in ice stress and indirectly by validating trends in reanalysis wind stress. The ice-motion trends suggest that increased cyclonic forcing has accelerated the Ross Gyre, supporting its possible involvement in ice-sheet melting and Ross Sea freshening[24]. The decrease in Weddell Sea ice cyclonicity suggests a Weddell Gyre deceleration, implying that gyre changes alone cannot explain the warming of Antarctic Bottom Water exported to the abyssal Atlantic[25]. Changes in meridional ice

export also affect freshwater budgets, implying greater brine release in the southern Ross[16,17] and King Håkon seas and increased meltwater input to their north, which may have contributed to the freshening of Antarctic Intermediate Water[26]. The data presented here thus offer a new observational insight into many facets of the Antarctic climate system.

Methods

We produced a data set of over 5 million individual ice-motion vectors on a 100-km polar stereographic grid by tracking brightness-temperature patterns in successive daily images from Special Sensing Microwave/Imager (SSMI) instruments[16,27]. Specifically, we used the 85 GHz vertically polarized channels of the SSMI instruments aboard satellites F8, F11, F13 and F17 of the Defense Meteorological Satellites Program. Supporting analyses used NASA (National Aeronautics and Space Administration) Team SSMI-derived ice concentrations[28] (http://nsidc.org/data/nsidc-0051.html) and the ERA-Interim atmospheric reanalysis (http://data-portal.ecmwf.int/data/d/interim_daily/) for the same period. Differences between the ice-motion data and analyses from higher-resolution satellite data and *in situ* buoys have mean 0–0.5 cm s^{-1} and standard deviation 4–8 cm s^{-1} (refs 27,29), levels of accuracy consistent with similar data sets[13]. SSMI ice-concentration data are accurate to approximately 5% for the winter measurements presented here[28].

We restrict our analyses to only the period of continuous daily sampled 85 GHz data, 1992–2010, producing a consistently sampled and high-quality record that allows the unambiguous identification of long-term trends. The motion-tracking procedure is less accurate when the ice is experiencing surface melt, causing more ice-motion data to be rejected during summer months, so to ensure a consistent coverage we use only data from April–October. Data are also often missing near the ice edge, because fast day-to-day changes in ice features are not resolvable by the tracking procedure. These seasonal and spatial limitations imply that our conclusions are limited to the behaviour of only the internal ice pack, away from the ice edge, and only in non-summer months. This is an important limitation because recent studies suggest that the Antarctic trends are related to modulation of the advance and retreat of the ice edge by summertime interaction with the ocean[9].

Interannual trends at each grid point are calculated from yearly averages that are taken over either the whole observation period in each year (April–October) or only from autumn data, defined here as April–June to maximize the use of our data. A fraction of the annual ice advance (and its trends) occurs earlier in the year in some regions[9], for which we have insufficient data. Trends are calculated separately for each component of a vector, and these vector trends are then plotted. The significance of a vector trend is itself a vector, which complicates its illustration in figures. We choose to highlight the significance of trends only in the meridional direction, because trends in northward ice export generally have the most important impacts.

The field of vector correlations presented in Fig. 1b is designed to quantify the linkage between interannual trends in winds and ice motion, so April–October daily vectors in each quantity are first averaged into yearly means, and then the 19-year time series of ice motion and wind vectors are correlated at each grid point. The relationship between time series of wind and ice-drift vectors is examined using a vector correlation measure that can be viewed as a generalization of the simple correlation coefficient between two scalar time series[30]. According to the method, the two vector time series at each grid point would be perfectly correlated if the magnitude of the vectors were related by a constant factor and their direction subject to a constant offset. The resulting r^2 is scaled to lie between 0 and 1 here for ease of comparison with scalar correlation values. If the two vector series are independent, nr^2 is asymptotically distributed as χ^2 with four degrees of freedom, but for smaller samples ($n \ll 64$) its distribution can be calculated empirically[30]. This can be used to assess the significance of correlations; for $n = 19$ and using r^2 scaled to lie between 0 and 1 we estimate that a correlation of $r^2 = 0.4$ provides a significance level of 99% (ref. 30).

Received 13 April 2012; accepted 9 October 2012; published online 11 November 2012

References

1. Zwally, H. J., Comiso, J. C., Parkinson, C. L., Cavalieri, D. J. & Gloersen, P. Variability of Antarctic sea ice 1979–1998. *J. Geophys. Res.* **107,** 3041 (2002).
2. Comiso, J. C. & Nishio, F. Trends in the sea ice cover using enhanced and compatible AMSR-E, SSM/I, and SMMR data. *J. Geophys. Res.* **113,** C02s07 (2008).
3. Liu, J. P., Curry, J. A. & Martinson, D. G. Interpretation of recent Antarctic sea ice variability. *Geophys. Res. Lett.* **31,** L02205 (2004).
4. Turner, J. *et al.* Non-annular atmospheric circulation change induced by stratospheric ozone depletion and its role in the recent increase of Antarctic sea ice extent. *Geophys. Res. Lett.* **36,** L08502 (2009).
5. Lefebvre, W. & Goosse, H. Influence of the Southern Annular Mode on the sea ice-ocean system: The role of the thermal and mechanical forcing. *Ocean Sci.* **1,** 145–157 (2005).
6. Liu, J. P. & Curry, J. A. Accelerated warming of the Southern Ocean and its impacts on the hydrological cycle and sea ice. *Proc. Natl Acad. Sci. USA* **107,** 14987–14992 (2010).
7. Manabe, S., Spelman, M. J. & Stouffer, R. J. Transient responses of a coupled ocean atmosphere model to gradual changes of atmospheric CO_2. Part II: Seasonal response. *J. Clim.* **5,** 105–126 (1992).
8. Jacobs, S. S. & Comiso, J. C. Climate variability in the Amundsen and Bellingshausen Seas. *J. Clim.* **10,** 697–709 (1997).
9. Stammerjohn, S. E., Massom, R., Rind, D. & Martinson, D. G. Regions of rapid sea ice change: An inter-hemispheric seasonal comparison. *Geophys. Res. Lett.* **39,** L06501 (2012).
10. Zhang, J. L. Increasing Antarctic sea ice under warming atmospheric and oceanic conditions. *J. Clim.* **20,** 2515–2529 (2007).
11. Eisenman, I., Schneider, T., Battisti, D. S. & Bitz, C. M. Consistent changes in the sea ice seasonal cycle in response to global warming. *J. Clim.* **24,** 5325–5335 (2011).
12. Emery, W. J., Fowler, C. W. & Maslanik, J. A. Satellite-derived maps of Arctic and Antarctic sea ice motion: 1988–1994. *Geophys. Res. Lett.* **24,** 897–900 (1997).
13. Heil, P., Fowler, C. W. & Lake, S. E. Antarctic sea-ice velocity as derived from SSM/I imagery. *Ann. Glaciol. Ser.* **44,** 361–366 (2006).
14. Kimura, N. Sea ice motion in response to surface wind and ocean current in the Southern Ocean. *J. Meteorol. Soc. Jpn* **82,** 1223–1231 (2004).
15. Lefebvre, W., Goosse, H., Timmermann, R. & Fichefet, T. Influence of the Southern Annular Mode on the sea ice-ocean system. *J. Geophys. Res.* **109,** C09005 (2004).
16. Comiso, J. C., Kwok, R., Martin, S. & Gordon, A. L. Variability and trends in sea ice extent and ice production in the Ross Sea. *J. Geophys. Res.* **116,** C04021 (2011).
17. Drucker, R., Martin, S. & Kwok, R. Sea ice production and export from coastal polynyas in the Weddell and Ross Seas. *Geophys. Res. Lett.* **38,** L17502 (2011).
18. Comiso, J. C. *Polar Oceans from Space* (Springer, 2010).
19. Stammerjohn, S. E., Martinson, D. G., Smith, R. C., Yuan, X. & Rind, D. Trends in Antarctic annual sea ice retreat and advance and their relation to El Niño-Southern Oscillation and Southern Annular Mode variability. *J. Geophys. Res.* **113,** C03s90 (2008).
20. Kimura, N. & Wakatsuchi, M. Large-scale processes governing the seasonal variability of the Antarctic sea ice. *Tellus A* **63,** 828–840 (2011).
21. White, W. B. & Peterson, R. G. An Antarctic circumpolar wave in surface pressure, wind, temperature and sea-ice extent. *Nature* **380,** 699–702 (1996).
22. Yuan, X. J. & Li, C. H. Climate modes in southern high latitudes and their impacts on Antarctic sea ice. *J. Geophys. Res.* **113,** C06s91 (2008).
23. Thompson, D. W. J. *et al.* Signatures of the Antarctic ozone hole in Southern Hemisphere surface climate change. *Nature Geosci.* **4,** 741–749 (2011).
24. Jacobs, S. S., Giulivi, C. F. & Mele, P. A. Freshening of the Ross Sea during the late 20th century. *Science* **297,** 386–389 (2002).
25. Meredith, M. P. *et al.* Synchronous intensification and warming of Antarctic Bottom Water outflow from the Weddell Gyre. *Geophys. Res. Lett.* **38,** L03603 (2011).
26. Wong, A. P. S., Bindoff, N. L. & Church, J. A. Large-scale freshening of intermediate waters in the Pacific and Indian oceans. *Nature* **400,** 440–443 (1999).
27. Kwok, R., Schweiger, A., Rothrock, D. A., Pang, S. & Kottmeier, C. Sea ice motion from satellite passive microwave imagery assessed with ERS SAR and buoy motions. *J. Geophys. Res.* **103,** 8191–8214 (1998).
28. Cavalieri, D. J., Parkinson, C. L., Gloersen, P & Zwally, H. J. *Sea Ice Concentrations from Nimbus-7 SMMR and DMSP SSM/I-SSMIS Passive Microwave Data, 1992–2010* (National Snow and Ice Data Center, 1996).
29. Kwok, R. Ross Sea ice motion, area flux, and deformation. *J. Clim.* **18,** 3759–3776 (2005).
30. Crosby, D. S., Breaker, L. C. & Gemmill, W. H. A proposed definition for vector correlation in geophysics—theory and application. *J. Atmos. Ocean. Technol.* **10,** 355–367 (1993).

Acknowledgements

Part of this work was performed at the Jet Propulsion Laboratory, California Institute of Technology, under contract with the National Aeronautics and Space Administration.

Author contributions

P.R.H. designed and performed the research and wrote the manuscript. R.K. provided the data and contributed to the manuscript.

Additional information

Supplementary information is available in the online version of the paper. Reprints and permissions information is available online at www.nature.com/reprints. Correspondence and requests for materials should be addressed to P.R.H.

Competing financial interests

The authors declare no competing financial interests.

nature geoscience
SUPPLEMENTARY INFORMATION
DOI: 10.1038/NGEO1627

Supplementary Information to "Wind-driven trends in Antarctic sea-ice motion" by

Paul R. Holland and Ron Kwok

Supplementary Methods

Combining ice motion and concentration data allows us to quantify the different processes contributing to the ice concentration budget. The evolution of ice concentration, A, is governed by

$$\frac{\partial A}{\partial t} + \nabla.(\boldsymbol{u}A) = f - r,$$

where $\boldsymbol{u}$ is ice motion, f is the ice concentration change from freezing or melting, and r is the concentration change from mass-conserving mechanical ice redistribution processes, such as ridging, that convert ice area to ice thickness. The results show that redistribution is generally small compared to freezing and melting (see below) so it is neglected here.

Rearranging and integrating over a particular time period, we obtain

$$A(t_2) - A(t_1) = \int_{t_1}^{t_2} f\, dt - \int_{t_1}^{t_2} \boldsymbol{u}.\nabla A\, dt - \int_{t_1}^{t_2} A\nabla.\boldsymbol{u}\, dt,$$

so the ice concentration difference between the end and start of any period is caused by the integrated contributions of freezing, advection, and divergence over that period. In this study the difference term on the left-hand side is calculated between 14-day means of ice concentration data centred upon the end and start of each period. Next, advection and divergence terms are calculated by integrating the relevant daily ice concentration and motion data over the period. Finally, the integrated freezing is determined from the residual of these other terms. We can only calculate these terms for the internal ice pack because the tracking procedure typically fails to capture motion near the ice edge. The formal error in these terms propagates from the quantified error in ice concentration and motion, and in theory is

DOI: 10.1038/NGEO1627

possible to calculate explicitly, but the assumptions required to calculate these errors (specifically the neglect of covariance) are so restrictive as to nullify the utility of the results.

To obtain an overview of the processes contributing to the mean Antarctic ice concentration balance, each of these four terms is calculated for each year and then averaged over our 19-year record

$$\overline{\Delta A} = \overline{\int f} - \overline{\int \boldsymbol{u}.\nabla A} - \overline{\int A\nabla.\boldsymbol{u}},$$

as discussed in the main text. Mean values of the four terms are shown for the whole year (April-October) in Supplementary Figure 1 and for autumn only (April-June) in Supplementary Figure 2. This approach shares some features with a previous method[20]. Passive microwave sea ice data have poorly-quantified seasonal biases (e.g. overestimating ice concentration in summer) that limit the quantitative accuracy of these results[28], but their qualitative overview is extremely infomative.

The 'freezing' term (e.g. Supplementary Figure 1d) is actually the calculation residual and also contains the effects of mechanical redistribution, but it is obvious from the results that it is dominated by thermodynamic processes. The term is generally positive in our non-summer data (an ice concentration source), which clearly represents freezing because it would otherwise require unobserved mechanical processes that convert thick to thin ice. Its negative regions (ice concentration sinks) primarily occur around the ice edge, where ice concentrations are low (< 0.5). When concentrations are low, ice convergence causes concentration to increase, as observed here (Supplementary Figure 1c), rather than decrease through ridging. Therefore we interpret the negative residual around the ice edge as melting, confirming that the residual is mainly thermodynamic. Mechanical processes contribute

significantly to the residual only in the small ice concentration sinks in the western Weddell and Ross seas, where there is strong ice convergence and full ice cover.

With our new 19-year record of ice motion, we can also use this decomposition method to investigate the contribution of dynamic and thermodynamic processes to the observed ice concentration trends. The value of each of the four terms is calculated for each year in our timeseries, and we then calculate the linear trends of these annual values over the 19-year time period τ

$$\frac{\partial\, \Delta A}{\partial \tau} = \frac{\partial \int f}{\partial \tau} - \frac{\partial \int \boldsymbol{u}.\nabla A}{\partial \tau} - \frac{\partial \int A \nabla.\boldsymbol{u}}{\partial \tau}.$$

Trends in autumn (April-June) data are plotted in Supplementary Figure 3 and discussed in the main text. We can then examine the proportional contribution of dynamic processes to the ice concentration trends by considering the ratio between trends in flux divergence (the sum of advection and divergence) and trends in ice concentration difference

$$D = -\frac{\partial \int \nabla.(\boldsymbol{u}A)}{\partial \tau} \Big/ \frac{\partial\, \Delta A}{\partial \tau}.$$

Supplementary Figure 4 shows these two fields and their ratio for our autumn data. Spatial offsets between the two fields lead to small-scale noise in their ratio. Extensive smoothing of the ratio reveals the spatial distribution of the importance of dynamic trends, as discussed in the main text.

DOI: 10.1038/NGEO1627

Supplementary Figures

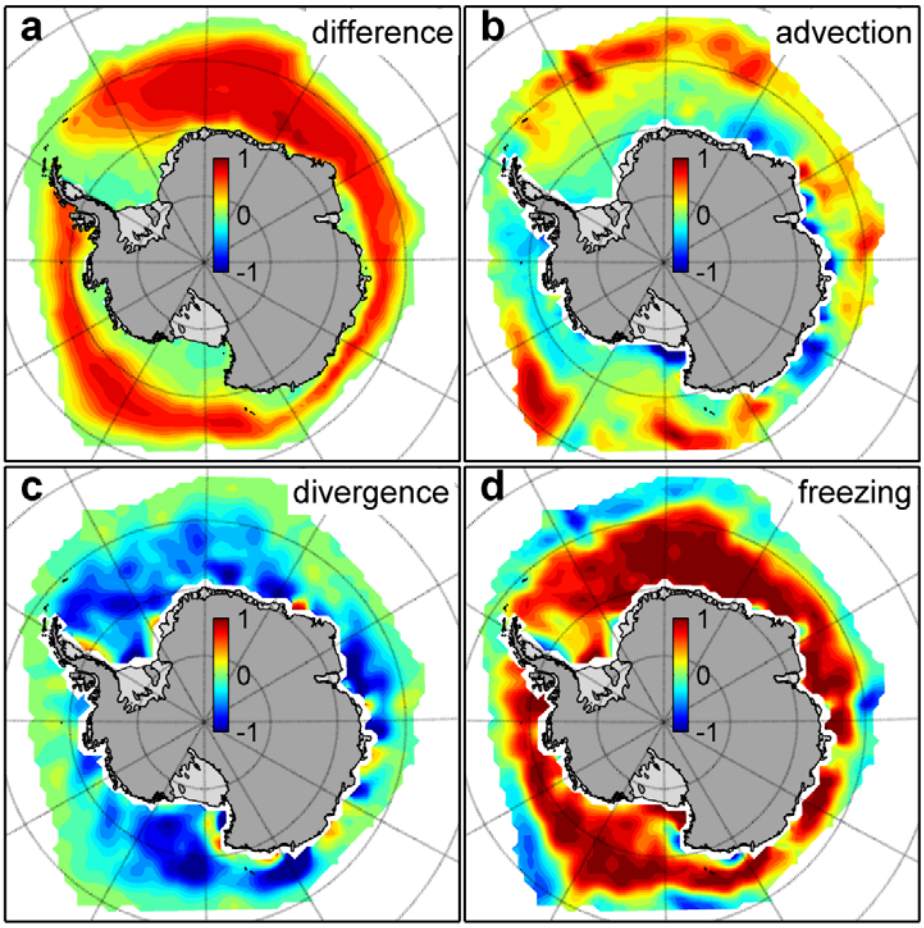

Supplementary Figure 1 | April-October 1992-2010 mean of each component in the ice concentration budget, showing divergence-maintained freezing close to Antarctica and advection-led melting around the ice margins. a) mean observed April-October ice concentration difference, $\overline{\Delta A}$; b) mean concentration difference from observed ice advection, $-\overline{\int \boldsymbol{u}.\nabla A}$; c) mean concentration difference from observed ice divergence, $-\overline{\int A\nabla.\boldsymbol{u}}$; d) mean concentration difference from residual freezing, $\overline{\int f}$. The ice concentration difference in panel a is comprised of the processes in panels b-d. Panels b-d have been smoothed with a 3-point mean to reduce grid-scale noise in the derivatives.

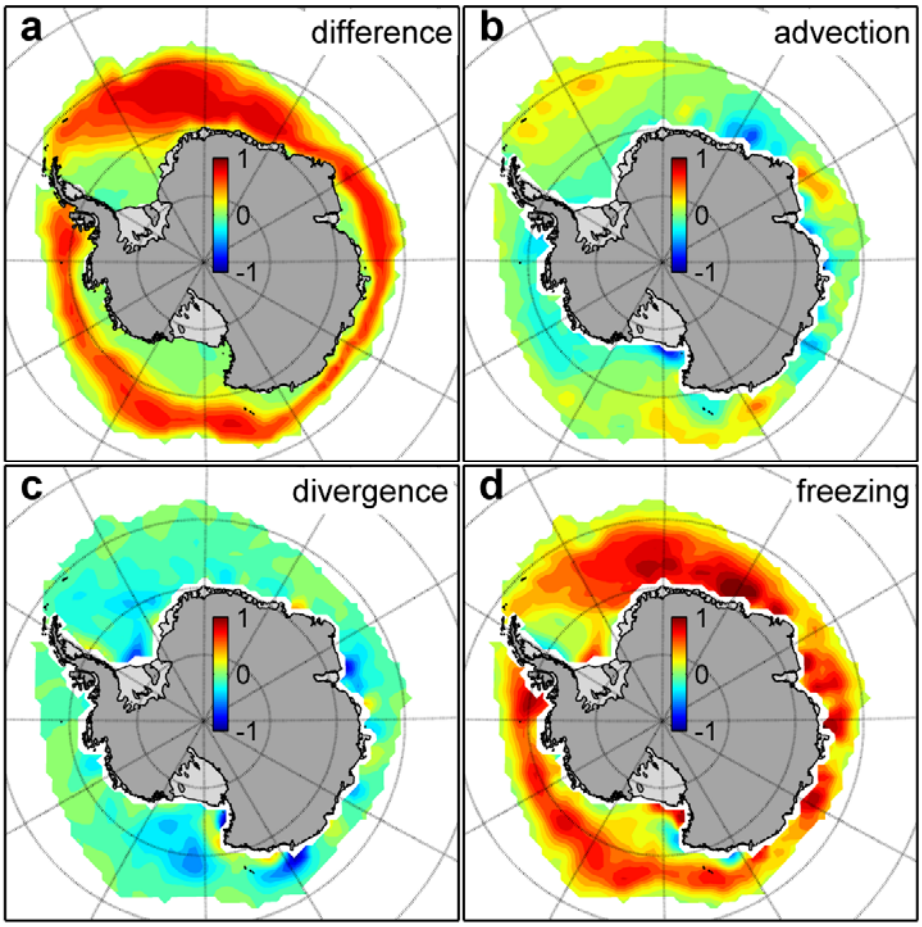

Supplementary Figure 2 | Autumn (April-June) 1992-2010 mean of each component in the ice concentration budget, showing that ice growth is dominated by thermodynamics during this period. Panels calculated as described in Supplementary Figure 1.

DOI: 10.1038/NGEO1627

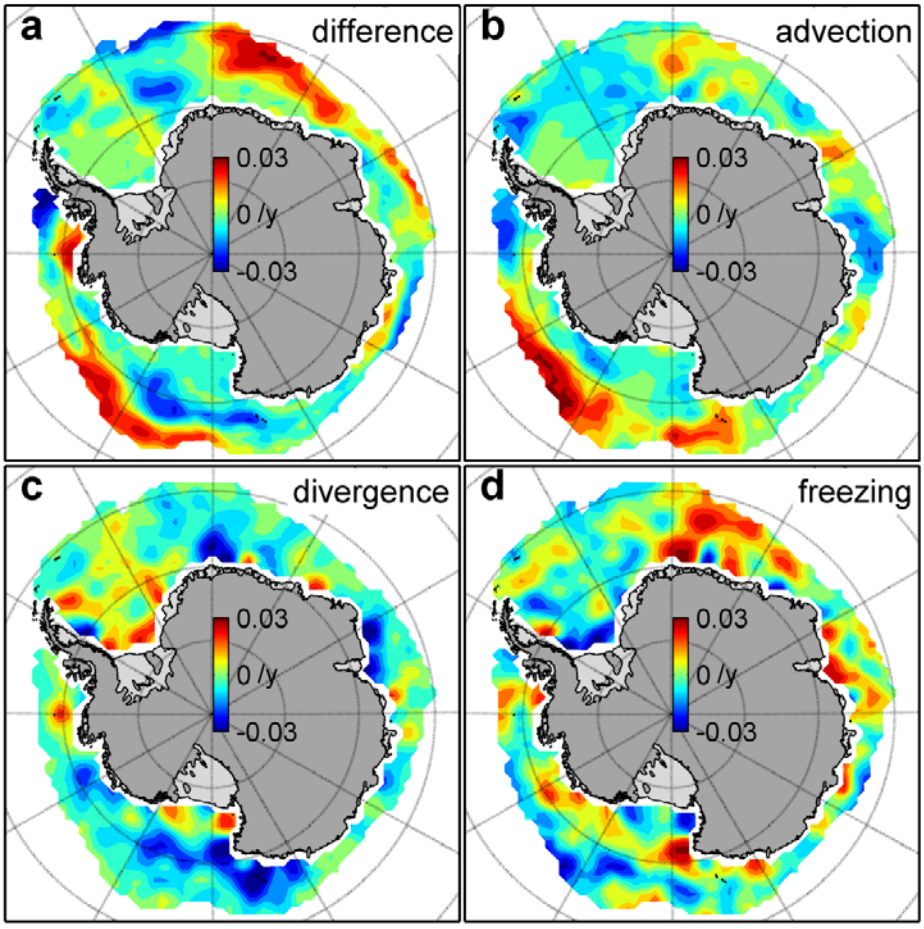

Supplementary Figure 3 | Autumn (April-June) 1992-2010 trends in all components of the ice concentration budget, quantifying the contribution of trends in dynamic and thermodynamic processes to the overall ice concentration trends. a) trend in observed April-June ice concentration difference, $\partial \Delta A/\partial \tau$; b) trend in concentration difference from observed advection, $-\partial \int \boldsymbol{u}.\nabla A/\partial \tau$; c) trend in concentration difference from observed divergence, $-\partial \int A\nabla.\boldsymbol{u}/\partial \tau$; d) trend in concentration difference from residual freezing, $\partial \int f/\partial \tau$; The trend in ice concentration difference shown in panel a is comprised of the trends in the processes shown in panels b-d. Panels b-d have been smoothed with a 3-point mean to reduce grid-scale noise in the derivatives.

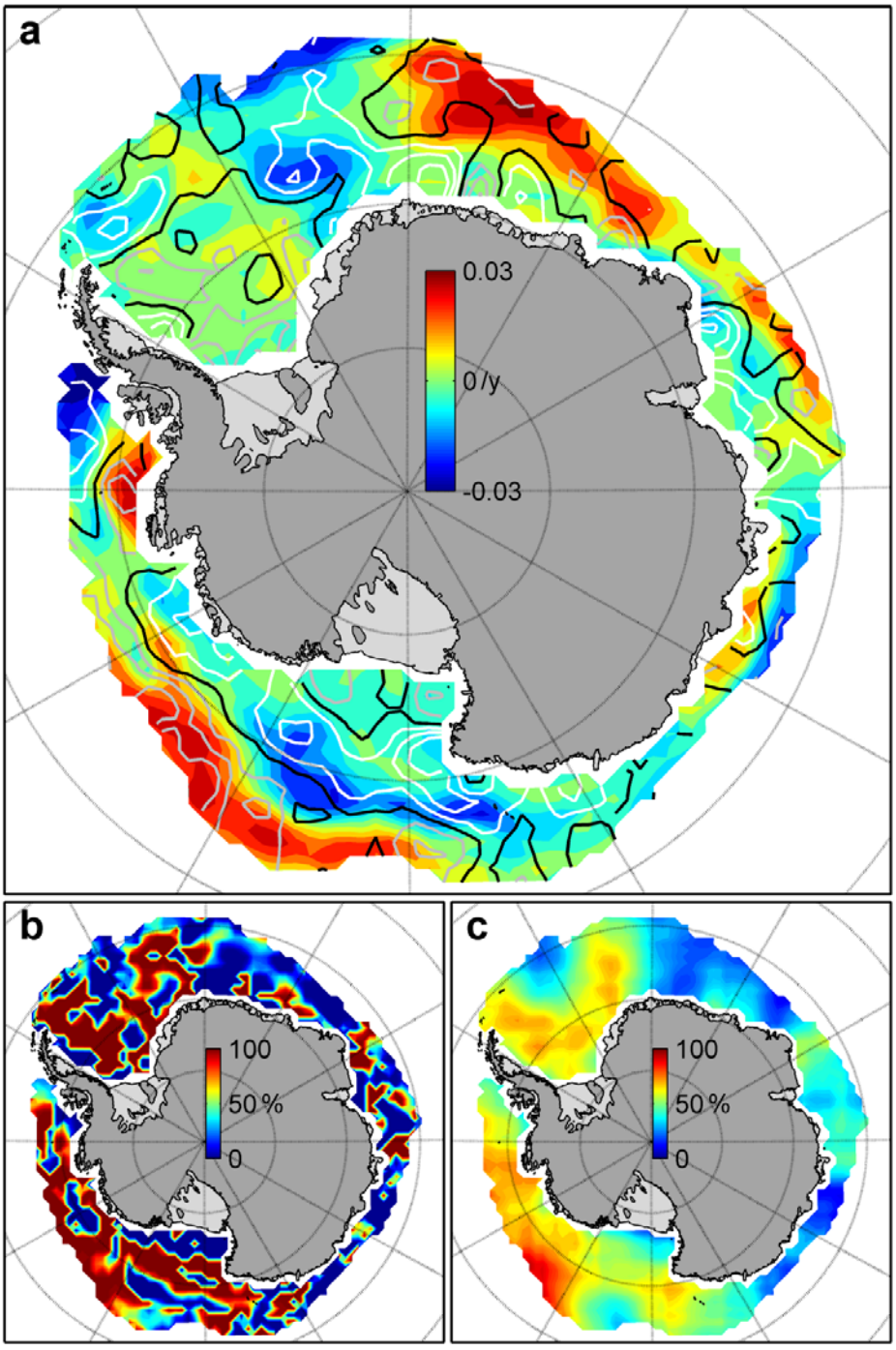

Supplementary Figure 4 | The relation between trends in autumn concentration difference from flux divergence (the sum of advection and divergence) and total trends in autumn ice concentration difference. Extensive smoothing of their ratio reveals a general dominance of dynamic trends in the Pacific sector and Weddell Sea and thermodynamic trends elsewhere. a) trend in ice concentration difference, $\partial \Delta A / \partial \tau$ (underlay), and trend in ice concentration

DOI: 10.1038/NGEO1627

difference from flux divergence, $-\partial \int \nabla.(\boldsymbol{u}A)/\partial\tau$ (overlay; black contour is zero trend, white contours are negative trends, grey contours are positive trends, contour increment 0.01/y); b) unsmoothed fraction of ice difference trend that is explained by the trend in ice difference from flux divergence; c) as panel b but smoothed with a 7-point mean filter.